Evaluation of Small-Scale Laterally Loaded Non-Slender Monopiles in Sand

Roesen, Hanne Ravn; Thomassen, Kristina; Sørensen, Søren Peder Hyldal; Ibsen, Lars Bo

Publication date:
2010

Document Version
Publisher's PDF, also known as Version of record

Evaluation of Small-Scale Laterally Loaded Non-Slender Monopiles in Sand

H. R. Roesen
K. Thomassen
S. P. H. Sørensen
L. B. Ibsen

ISSN 1901-726X
DCE Technical Report No. 91

AALBORG UNIVERSITY
Department of Civil Engineering

Aalborg University
Department of Civil Engineering
Division of Water and Soil

DCE Technical Report No. 91

Evaluation of Small-Scale Laterally Loaded Non-Slender Monopiles in Sand

by

H. R. Roesen
K. Thomassen
S. P. H. Sørensen
L. B. Ibsen

June 2010

Scientific Publications at the Department of Civil Engineering

Technical Reports are published for timely dissemination of research results and scientific work carried out at the Department of Civil Engineering (DCE) at Aalborg University. This medium allows publication of more detailed explanations and results than typically allowed in scientific journals.

Technical Memoranda are produced to enable the preliminary dissemination of scientific work by the personnel of the DCE where such release is deemed to be appropriate. Documents of this kind may be incomplete or temporary versions of papers—or part of continuing work. This should be kept in mind when references are given to publications of this kind.

Contract Reports are produced to report scientific work carried out under contract. Publications of this kind contain confidential matter and are reserved for the sponsors and the DCE. Therefore, Contract Reports are generally not available for public circulation.

Lecture Notes contain material produced by the lecturers at the DCE for educational purposes. This may be scientific notes, lecture books, example problems or manuals for laboratory work, or computer programs developed at the DCE.

Theses are monograms or collections of papers published to report the scientific work carried out at the DCE to obtain a degree as either PhD or Doctor of Technology. The thesis is publicly available after the defence of the degree.

Latest News is published to enable rapid communication of information about scientific work carried out at the DCE. This includes the status of research projects, developments in the laboratories, information about collaborative work and recent research results.

Published 2010 by
Aalborg University
Department of Civil Engineering
Sohngaardsholmsvej 57,
DK-9000 Aalborg, Denmark

Printed in Aalborg at Aalborg University

ISSN 1901-726X
DCE Technical Report No. 91

Evaluation of Small-Scale Laterally Loaded Non-Slender Monopiles in Sand

H. R. Roesen[1]; K. Thomassen[1]; S. P. H. Sørensen[2]; and L. B. Ibsen[3]

Aalborg University, June 2010

Abstract

In current design of offshore wind turbines, monopiles are often used as foundation. The behaviour of the monopiles when subjected to lateral loading has not been fully investigated, e.g. the diameter effect on the soil response. In this paper the diameter effect on laterally loaded non-slender piles in sand is evaluated by means of results from six small-scale laboratory tests, numerical modelling of the same test setup and existing theory. From the numerical models $p-y$ curves are conducted and compared to current design regulations. It is found that the recommendations in API (1993) and DNV (1992) are in poor agreement with the numerically obtained $p-y$ curves. The initial stiffness, E^*_{py}, of the $p-y$ curves, is found to be dependent on the pile diameter, i.e. the initial stiffness increases with increasing pile diameter. Further, the dependency is found to be in agreement with the suggestions in Sørensen et al. (2010). It is found that considerable uncertainties are related to small-scale testing, and the different evaluations clearly indicate that the accuracy of small-scale testing is increased when increasing the pile diameter and applying overburden pressure.

1 Introduction

In the design of laterally loaded monopiles the $p-y$ curve method, given by the design regulations API (1993) and DNV (1992), is often used. For piles in sand the recommended $p-y$ curves are based on results from two slender, flexible piles with a slenderness ratio of $L/D = 34.4$, where L is the embedded length and D is the diameter of the pile. Contrary to the assumption of flexible piles for these curves the monopile foundations installed today have a slenderness ratio $L/D < 10$, and behave almost as rigid objects. The recommended curves does not take the effect of the slenderness ratio into account. Furthermore, the initial stiffness is considered independent of the pile properties such as the pile diameter. The research within the field of diameter effects gives contradictory conclusions. Different studies have found the initial stiffness to be either independent, linearly dependent, or non-linear dependent on the pile diameter, cf. Brødbæk et al. (2009).

The aim of this paper is to evaluate the diameter effect on the pile-soil interaction. Six small-scale tests on laterally loaded monopiles in sand have been conducted, cf. Thomassen et al. (2010). The diameter effect is evaluated by comparing results from these tests with calibrated numerical models of the same test setup and existing theory. Furthermore, $p-y$ curves

[1]Graduate Student, Dept. of Civil Engineering, Aalborg University, Denmark

[2]Professor, Dept. of Civil Engineering, Aalborg University, Denmark.

[3]PhD Fellow, Dept. of Civil Engineering, Aalborg University, Denmark.

recommended in the current design regulations API (1993) and DNV (1992) are compared to curves obtained from the numerical models. As the foundations for offshore wind turbines are sensitive towards rotation and vibrations, strict demands for the stiffness of the foundation are induced. Therefore, the diameter effect is evaluated with focus on the initial stiffness of the $p-y$ curves.

2 Laboratory Test Setup

Six quasi-static tests on two closed-ended aluminium piles with a wall-thickness of 5 mm and outer diameters of 40 mm and 100 mm, respectively, have been conducted. The piles had a slenderness ratio, L/D, of 5 corresponding to embedded lengths of 200 mm and 500 mm. The piles were installed in 580 mm fully saturated sand. The aim of the tests was to obtain load-deflection relationships for the piles. Therefore, the piles were loaded laterally 370 mm above the soil surface, and the deflection of the pile was measured at three levels, cf. Fig. 1.

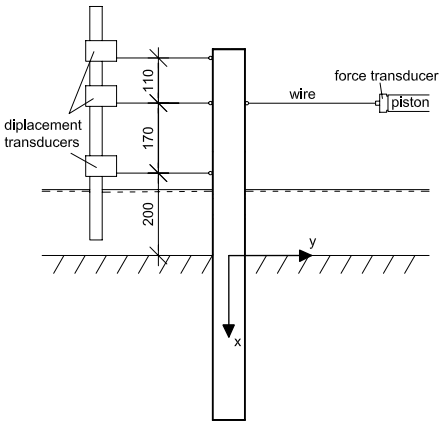

Figure 1: Setup for measuring the lateral deflection of the pile at three levels. The measurements are given in mm.

In order to minimize errors such as small non-measurable stresses and a non-linear failure criterion, the tests were conducted in the pressure tank shown in Fig. 2. The

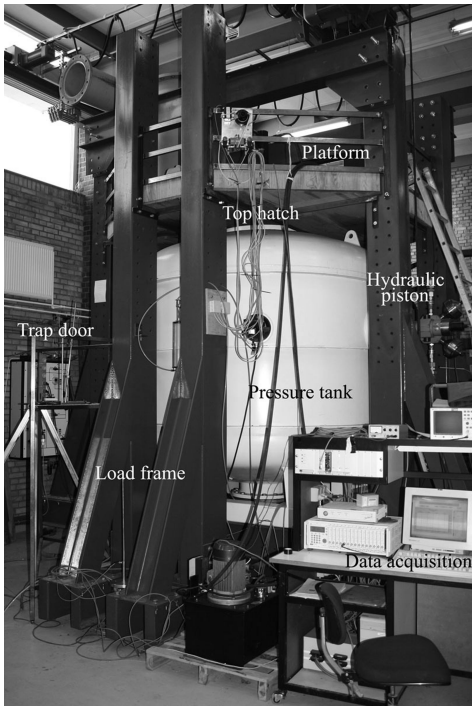

Figure 2: The pressure tank installed in the Geotechnical Engineering Laboratory at Aalborg University, Denmark.

effective stresses in the soil were increased by placing an elastic membrane on the soil surface sealing the soil from the upper part of the pressure tank. When increasing the pressure in the upper part of the tank the membrane was pressed against the soil leading to an increase of the stresses in the soil. The lower part of the tank was connected to an ascension pipe ensuring that the load was applied as contact pressures between the grains only, i.e. an increase of the effective stresses. The tests were conducted at stress levels of 0 kPa, 50 kPa, and 100 kPa.

The soil parameters were determined from cone penetration tests in accordance to Ibsen et al. (2009). A detailed description of the laboratory tests can be found in Thomassen et al. (2010).

3 Numerical 3D Models

The six laboratory tests are modelled in FLAC^{3D}, which is a commercial explicit finite difference program. Because of axis symmetry in the tests, only half the test setup is modelled. The modelling programme is chosen to match the testing programme in Thomassen et al. (2010), cf. Tab. 1.

Table 1: Modelling programme for the FLAC^{3D} models.

		D [mm]	L/D [-]	P_0 [kPa]
Model 1	(Test 1)	100	5	0
Model 2	(Test 2)	100	5	50
Model 3	(Test 3)	100	5	100
Model 4	(Test 4)	40	5	0
Model 5	(Test 5)	40	5	50
Model 6	(Test 6)	40	5	100

The generation of the models and the finite difference calculations are carried out stepwise as described in the following.

3.1 Geometry of the 3D Models

The model geometry is set to match the condition in the pressure tank. Therefore, the outer boundaries are given as the volume of the soil mass in the tank, i.e. a diameter of 2.1 m and a soil depth of 0.58 m. The soil and pile are generated by use of predefined zone elements to which different material models and properties can be assigned. Each zone element is automatically discritised into five tetrahedron subelements, which are first order, constant rate of strain elements. Because large variations in strain and stresses occur in the soil near the pile a finer zone mesh is generated in this area.

In order to model a correct pile-soil interaction an interface is generated between the pile and the soil by use of standard FLAC^{3D} interface elements. The elements are triangular and by default two interface elements are generated for each zone face. The interfaces are one-sided and attached to the soil. The constitutive model for the interface is defined by a linear Coulomb shear-strength criterion that limits the shear force acting at an interface node after the shear strength limit is reached.

Firstly, the soil is generated, secondly, the interface is generated and attached to the soil elements and, thirdly, the pile is generated. Initially, the pile grid is generated separately and later moved into the soil and in contact with the interface. Hereby, it is possible to group the pile elements and specify pile nodes for the computation of bending moment. As a simplification, the piles are modelled as solid cylinders in contrast to the closed-ended pipe piles used in the laboratory tests. The solid piles are modelled with a reduced modulus of elasticity and reduced density based on equivalence with the pipe piles used in the laboratory tests, cf. Sec. 3.5. The zone geometry for the 100 mm pile is shown in Fig. 3. In Sørensen et al. (2009) convergence analyses were conducted and the geometries used in this article are in agreement with the analyses. Note that the shown coordinate system is in agreement with the coordinate system employed for laterally loaded piles in the design regulations and does not represent the system used in FLAC^{3D}.

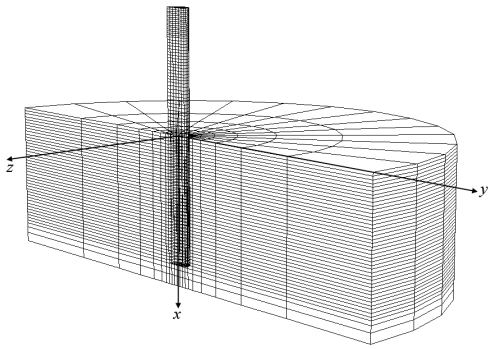

Figure 3: Zone geometry in the models with the 100 mm pile.

3.2 Boundary and Initial Conditions

When the geometry is generated the boundary and initial conditions are assigned. At the outer perimeter of the soil the element nodes are restrained in the y- and z-direction, cf. Fig. 3. At the bottom surface of the model the nodes are restrained in all directions. Because only half the laboratory setup is modelled the nodes at the symmetry line are restrained in the z-direction.

The initial stresses are initialised based on the density of the material, the gravitational loading, and the overburden pressure. The horizontal stresses are generated by use of a K_0-procedure in which $K_0 = 1 - \sin\varphi_{tr}$.

3.3 Calculation Phase

In order to prevent stress concentrations near the pile the model is brought to equilibrium with both the pile and the soil having the material properties of the soil. Further, the pile is assumed smooth by setting the interface friction equal to zero. Hereafter, the pile and interface are assigned the material properties for the pile and interface, respectively, cf. Sec. 3.5. Again, the model is brought to equilibrium. This second equilibrium ensures a correct generation of the initial interface stresses. When equilibrium is reached all displacements are reset to zero.

The lateral load is applied as lateral velocities at $x = -370$ mm. The velocities are applied to the nodes at the centre of the pile corresponding to $y = 0$. Hereby, no additional bending moment is introduced in the pile. In order to avoid a dynamic response of the system the velocity is applied in small increments.

During the calculations the total lateral force, H, the displacement, y, and the stresses, σ, along the pile are recorded. The bending moment, M, and soil pressure, p, are calculated based on the recorded stresses in the pile and the interface, respectively, cf. Sec. 3.6.

3.4 Material Models

To describe the constitutive relations in the soil an elasto-plastic Mohr-Coulomb model is employed. As the soil is considered cohesionless no tension forces are allowed. Thus, tension cut-off is employed in the model. The yield function of the model defines the stress for which plastic flow takes place and is controlled by a non-associated flow rule. The piles are modelled by use of an elastic, isotropic model.

3.5 Material and Interface Properties

The soil properties in the six models are defined equal to the findings of the six laboratory tests, cf. Tab. 2. (Thomassen et al., 2010)

Table 2: Soil properties determined by the six laboratory tests and employed in the FLAC^{3D} models. The elasticity moduli written in parentheses are found by means of the numerical model.

	φ_{tr} [°]	ψ_{tr} [°]	γ' [kN/m^3]	E_0 [MPa]
Model 1	53.7	19.6	10.3	(4.0)
Model 2	50.3	19.0	10.4	38.24
Model 3	47.7	18.3	10.4	55.61
Model 4	54.4	20.4	10.4	(2.0)
Model 5	50.4	19.1	10.4	38.6
Model 6	48.0	18.6	10.4	57.2

For the tests without overburden pressure the low stresses lead to large uncertainties in the calculation of the initial tangential elasticity modulus, E_0. Thus, in the numerical models without overburden pressure E_0 is calibrated as described in Sec. 3.7. Due to the small variations in effective stresses through the soil layer the

soil parameters are assumed to be constant with depth for all the models. A cohesion, c, of 0.1 kPa and Poissons ratio, ν, of 0.23 are applied for the soil in all six models.

Because the piles are modelled as solid cylinders instead of hollow piles, as the ones used in the laboratory, an equivalent bending stiffness and density is required. Based on this equivalence a reduced elasticity modulus, E_{solid}, for the modelled piles are found.

$$E_{solid} = \frac{E_{hollow} \cdot I_{hollow}}{I_{solid}} \tag{1}$$

I is the second moment of inertia, and the subscripts $_{hollow}$ and $_{solid}$ denote the parameters derived for the pipe piles in the laboratory tests and the parameters employed in FLAC^{3D}, respectively. In the same way the density is equated with the cross-sectional area. The elasticity modulus and density of the pipe piles are set to the values for aluminium; $7.2 \cdot 10^4$ MPa and 2700 kg/m^3, respectively.

The interface properties are calibrated by means of the numerical models as described in Sec. 3.7. When using the interface properties listed in Tab. 3 the load-deflection curves are found to be similar to the curves obtained in the laboratory tests.

Table 3: Interface properties calibrated by means of the numerical models. E_0 is the initial tangential elasticity modulus of the soil, cf. Tab. 2.

Friction	φ_{int}	30°
Cohesion	c_{int}	0.1 kPa
Dilation	ψ_{int}	0°
Normal stiffness	k_n	$100 \times E_0$
Shear stiffness	k_s	$100 \times E_0$

3.6 Calculation of the Pile Bending Moment and Soil Resistance

The bending moment of the pile at a given level is calculated by use of Naviers formula, Eq. 2. In order to eliminate the average vertical stress, corresponding to the axial force acting on the pile, the bending moment in each level is calculated by two points $(y,z) = (\pm D/2, 0)$.

$$M = \frac{\sigma_{xx,i} \cdot I_{zz}}{y_i} \tag{2}$$

$\sigma_{xx,i}$ is the vertical normal stress at point i, I_{zz} is the second moment of inertia around the z-axis, and y_i is the y-coordinate for the point, cf. Fig. 3. The soil resistance per unit length along the pile, p_y, is computed directly by integrating the stresses in the interface nodes along the interface circumference C.

$$p_y = \int T_y dC \tag{3}$$

T_y is the y-component stress in a node i positioned in the interface.

3.7 Calibration of the Numerical Models

The calibration of the numerical models is based on a comparison between the modelled load-deflection curves and the load-deflection curves obtained from the small-scale tests in the laboratory.

For the models without overburden pressure E_0 is calibrated in relation to the initial stiffness of the load-deflection curves. In Figs. 4 and 5 the calibrated curves for $P_0 = 0$ kPa are shown. In the figures it is seen that the capacity of the calibrated models exceeds the capacity of the laboratory tests. This indicates that the internal angle of friction, φ_{tr}, inserted in the models is overestimated. φ_{tr} is based on the CPT's conducted prior to each laboratory test. At low stress levels φ_{tr} varies significantly with the stresses and it is difficult to determine φ_{tr} with sufficient accuracy.

The agreement between the capacity in the calibrated and the measured load-deflection relationship are found to increase with increasing pile diameter and

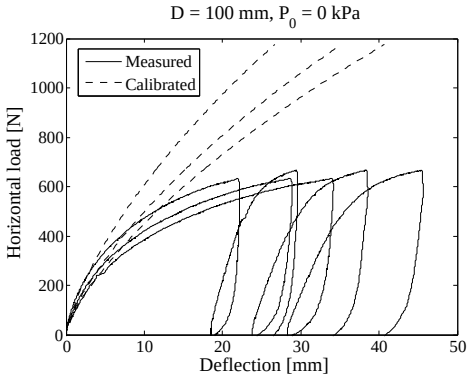

Figure 4: Calibrated and measured relationships at three levels above the soil surface for the test 100 mm with P_0 = 0 kPa.

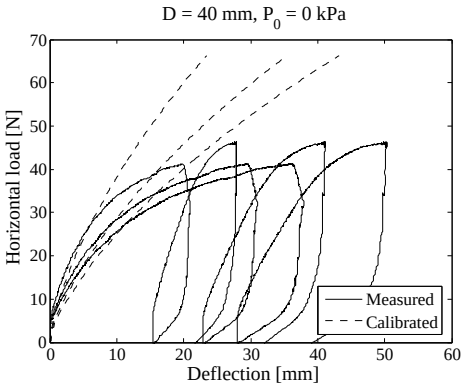

Figure 5: Calibrated and measured relationships at three levels above the soil surface for the 40 mm pile with P_0 = 0 kPa.

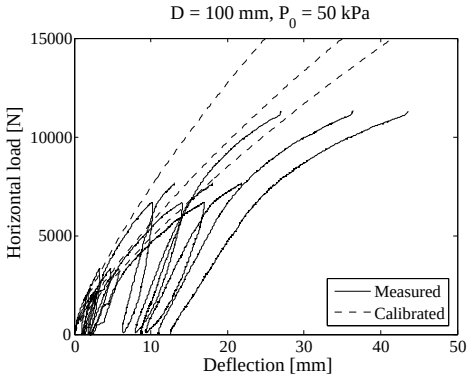

Figure 6: Calibrated and measured relationships at three levels above the soil surface for the 100 mm pile with P_0 = 0 kPa.

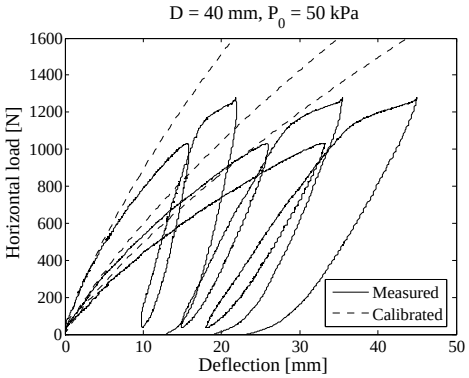

Figure 7: Calibrated and measured relationships at three levels above the soil surface for the 40 mm pile with P_0 = 0 kPa.

increasing overburden pressure, cf. Figs. 4 to 9. Thus, the best agreement is found for the 100 mm pile with an overburden pressure of 100 kPa, cf. Fig. 8.

Considerable uncertainties are related to the test results for the 40 mm pile, cf. Thomassen et al. (2010). This can also be concluded from the calibration of the model with the 40 mm pile and P_0 = 100 kPa as significant disagreement between the calibrated and the measured values are found, cf. Fig. 9. This disagreement is explained by a disturbance of the soil prior to the test as described in Thomassen et al. (2010).

The calibration of the six models clearly indicates that the accuracy in small-scale testing is increased when increasing the pile diameter and applying overburden pressure.

4 Evaluation of Results from the Numerical Models

Prior to the evaluation of the bending moment and deflection of the pile a convergence of the stresses in the numerical models is checked by a comparison between the

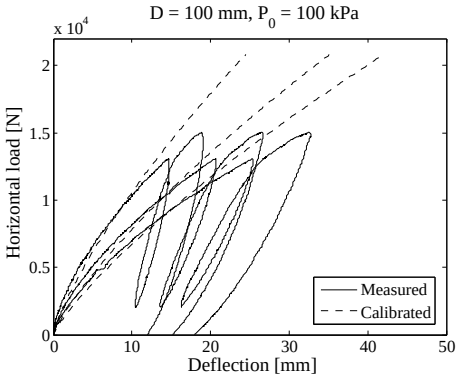

Figure 8: Calibrated and measured relationships at three levels above the soil surface for the 100 mm pile with P_0 = 100 kPa.

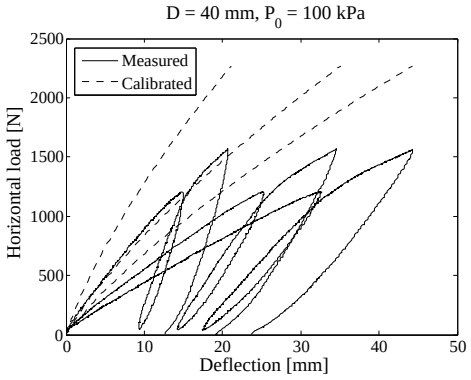

Figure 9: Calibrated and measured relationships at three levels above the soil surface for the 40 mm pile with P_0 = 100 kPa.

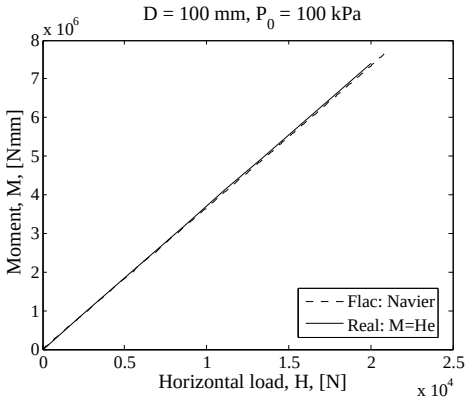

Figure 10: Comparison of the applied moment (applied load H multiplied with the load eccentricity, e, with the computed bending moment at soil surface for the 100 mm pile with P_0 = 100 kPa.

applied moment and the computed bending moment, cf. Fig. 10. In all the models the computed bending moment is in agreement with the applied moment.

4.1 Evaluation of Bending Moment and Lateral Deflection

In Figs. 11 and 12 the bending moment distribution along the piles below the soil surface is shown. For both models the prescribed displacement at $x = -370$ mm is 35 mm. In the figures it is seen that the maximum bending moment occurs at different locations depending on the overburden pressure. When overburden pressure is applied, the point of maximum bending moment is located closer to the soil surface. This indicates that the relative increase in soil resistance with overburden pressure is most significant at the soil surface.

In Figs. 13 and 14 the lateral deflection with depth at three different overburden pressures is shown. The prescribed deflection at $x = -370$ mm is 35 mm. Below the soil surface the deflection is recorded in 21 levels for the 40 mm pile and 26 levels for the 100 mm pile. Above the soil surface the deflection is recorded in two levels: $x = -200$ mm and $x = -370$ mm.

When applying overburden pressure the pile exhibits a more flexible behaviour than without overburden pressure, cf. Figs. 13 and 14. This is in accordance with Poulos and Hull (1989), who proposed a criterion for the pile-soil interaction in which an increase in the soil stiffness compared to the pile stiffness will lead to a more flexible behaviour of the pile. When applying overburden pressure the effective stress level increases, leading to an increase in the soil stiffness.

Although the piles behave more flexible when overburden pressure is applied, the primary deflection is caused by rigid body

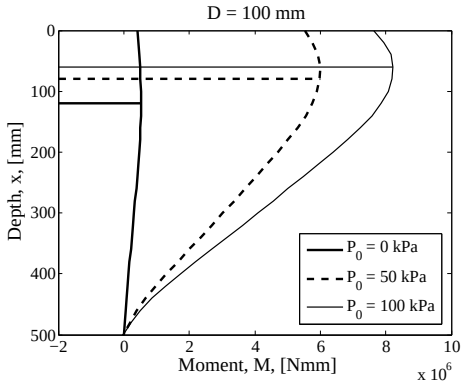

Figure 11: Bending moment distribution at different overburden pressures for the 100 mm piles. The horizontal lines indicate the depth of maximum moment.

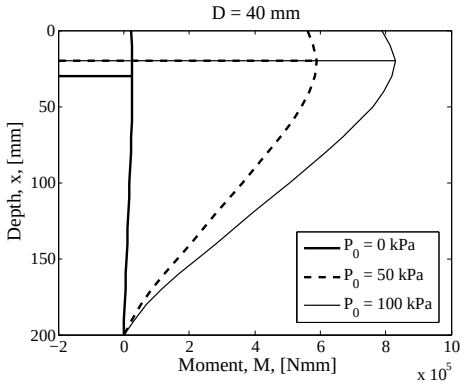

Figure 12: Bending moment distribution at different overburden pressures for the 40 mm piles. The horizontal lines indicate the depth of maximum moment.

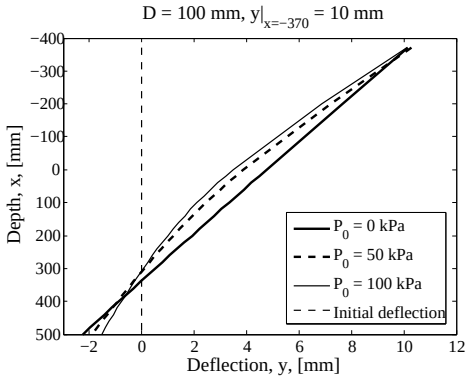

Figure 13: Lateral deflection with depth for different overburden pressures for the 100 mm piles.

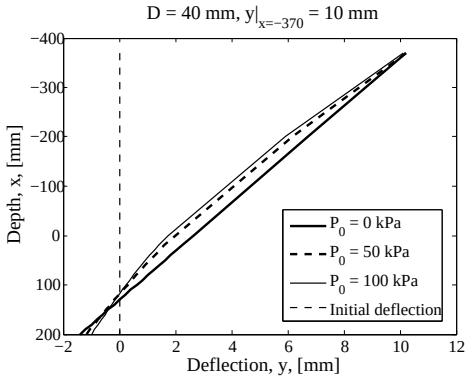

Figure 14: Lateral deflection with depth for different overburden pressures for the 40 mm piles.

rotation, which is evident because only a single point of rotation and a negative deflection at pile toe is present, cf. Figs. 13 and 14.

4.2 Evaluation of Diameter effect on the p–y Curves

The $p - y$ curves from the models with 40 mm and 100 mm piles without overburden pressures are compared at three different depths; 20 mm, 40 mm and 60 mm, cf. Fig. 15.

At the depth of 20 mm the ultimate soil resistance for the 100 mm pile is higher than for the 40 mm pile. At the depth of 40 mm the opposite is the case. For the depth of 60 mm it seems the curve for the 40 mm pile is approaching the ultimate soil resistance for the 100 mm pile. Which of the two curves that reaches the highest ultimate resistance is not possible to predict because of the limited displacement applied. Based on Fig. 15 the diameter is not thought to have a significant influence on the ultimate soil resistance.

From Fig. 15 it can be seen that the initial stiffness of the curves are dependent on the pile diameter, i.e. the larger pile diameter the higher initial stiffness. This is in contrast to API (1993) and DNV (1992) in which the initial stiffness is considered

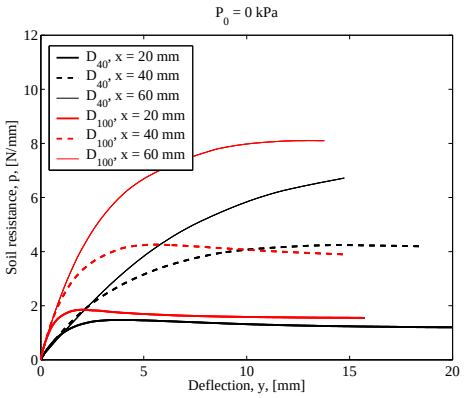

Figure 15: $p - y$ curves at three different depths for models with 40 mm and 100 mm piles and P_0 = 0 kPa.

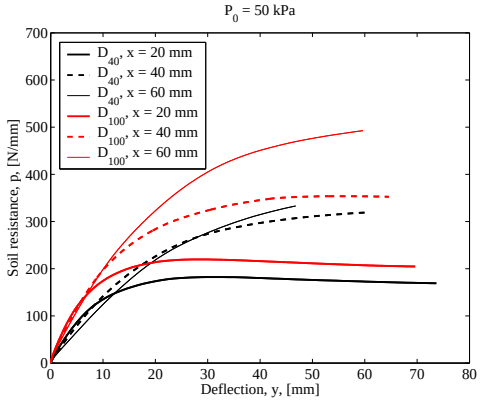

Figure 16: $p - y$ curves at three different depths for models with 40 mm and 50 mm piles and P_0 = 100 kPa

independent on the pile diameter. The dependency of the diameter on the initial stiffness is further evaluated in Sec. 7.

For the models with overburden pressure the three $p - y$ curves at same levels are shown in Figs. 16 and 17. As in the models without overburden pressure the initial stiffness of the $p - y$ curves is found to be dependent on the pile diameter.

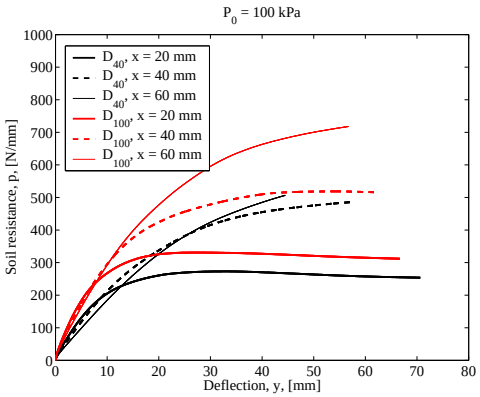

Figure 17: $p - y$ curves at three different depths for models with 40 mm and 100 mm piles and P_0 = 100 kPa.

4.3 Evaluation of the p–y Curves Dependency on Stress Level

In Figs. 18 to 20 the soil resistance along the 100 mm pile is shown for a prescribed deflection of 10 mm and 35 mm at $x = -370$ mm, respectively. The soil resistance is calculated at 24 levels along the pile and are shown for the pressures 0 kPa, 50 kPa, and 100 kPa. In Figs. 21 to 23 the $p-y$ curves for the 100 mm pile at the 24 levels are shown for the different overburden pressures. In the current theory concerning the initial stiffness, E^*_{py}, e.g. DNV (1992); API (1993); Lesny and Wiemann (2006); Sørensen et al. (2010), E^*_{py} is found to increase either linear or non-linear with depth. Therefore, the expected results from the obtained $p - y$ curves would be an increase in the E^*_{py} with depth as well.

Fig. 18 shows that the soil resistance increases with depth from the soil surface to a depth of approximately 150 mm. This increase is in agreement with the expected variation. When evaluating E^*_{py} of the $p - y$ curves in the same depth interval E^*_{py} is constant with depth, cf. Fig. 21. In the depth interval between 150 mm and the rotation point of the pile, at approximately 340 mm, the soil resistance is seen to decrease with depth. Concurrently, E^*_{py} is seen to decrease with depth in the same interval.

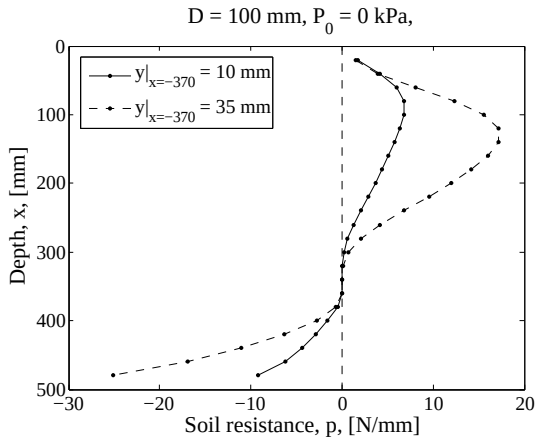

Figure 18: Soil resistance along the 100 mm pile with P_0 = 0 kPa.

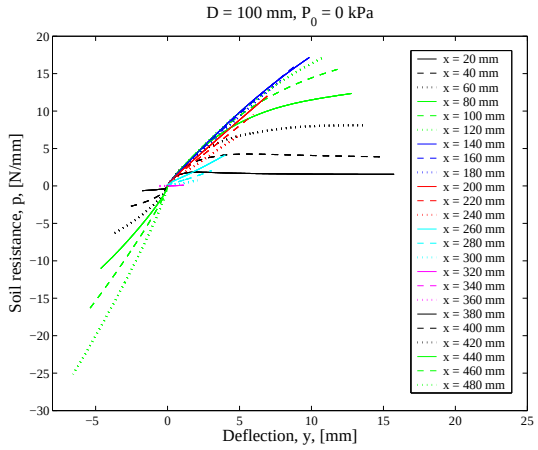

Figure 21: $p - y$ curves along the 100 mm pile with P_0 = 0 kPa.

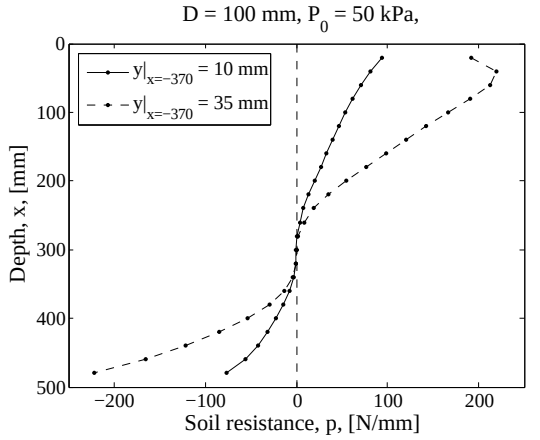

Figure 19: Soil resistance along the 100 mm pile with P_0 = 50 kPa.

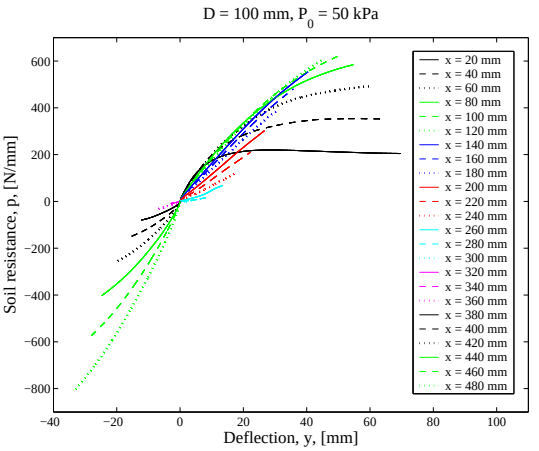

Figure 22: $p - y$ curves along the 100 mm pile with P_0 = 50 kPa.

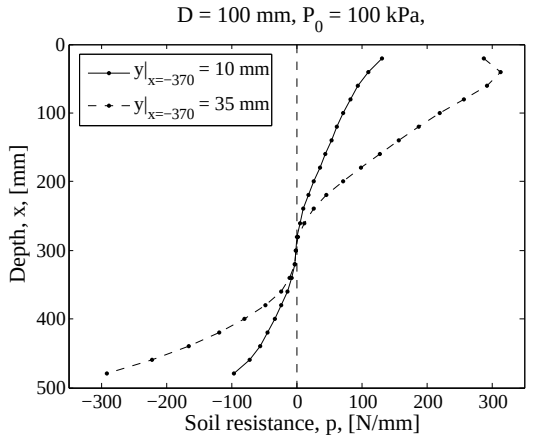

Figure 20: Soil resistance along the 100 mm pile with P_0 = 100 kPa.

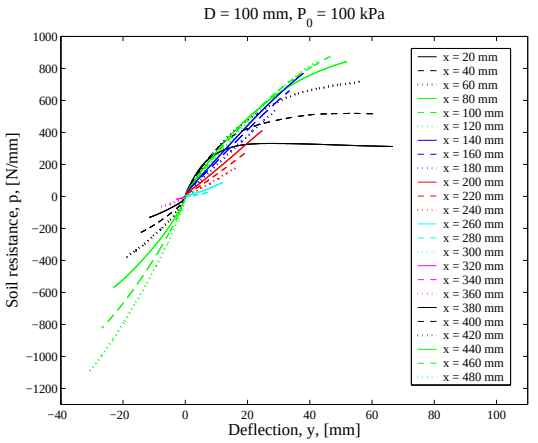

Figure 23: $p - y$ curves along the 100 mm pile with P_0 = 100 kPa.

Below the point of rotation, where the pile exhibit a negative deflection, a negative increase in the soil resistance is present. Below the point of pile rotation E^*_{py} is found to increase with depth.

In the models with overburden pressure, cf. Figs. 19 and 20, the soil resistance is mainly seen to decrease with depth from the soil surface to the point of pile rotation at approximately 310 mm. When evaluating the $p-y$ curves shown in Figs. 22 and 23 E^*_{py} is found to decrease with depth to the point of pile rotation. The soil resistance below the point of rotation is seen to increase negatively with depth and E^*_{py} increases. The findings imply that E^*_{py} is dependent on the state of stress. Similar findings are found when evaluating the 40 mm pile. At the point of no rotation the soil pressure is zero and it is therefore difficult to evaluate E^*_{py} near this point.

The obtained results should be considered with reservations due to the fact that the soil stiffness is modelled constant with depth. Secondly, a more advanced constitutive model, in which the variation of the stiffness with the deflection is taken into account, could have been used. Hereby, the stiffness of the soil would increase at small deflections, leading to an increase of the initial stiffness of the $p-y$ curves instead of the decrease of E^*_{py} at small deflections as observed in Figs. 18 to 23. Thus, in future research a further evaluation of E^*_{py} is recommended. The evaluation should consist of laboratory tests on piles instrumented with strain gauges, and numerical modelling with more advanced constitutive models employed.

5 Comparison of Test Results and Theory

To compare the test results to the recommendations given by the design regulations, API (1993) and DNV (1992), a traditional Winkler model is made in MATLAB by using the finite element toolbox CALFEM. Furthermore, the model is used to evaluate different expressions for the ultimate soil resistance.

5.1 Evaluation of Tests with Overburden Pressure

To model the tests with overburden pressure, P_0, the formulation for the ultimate soil resistance must be able to take P_0 into account. Hansen (1961) and Georgiadis (1983) both proposed a formulation in which the overburden pressure is taken into account. Hansen (1961) incorporated the overburden pressure directly in the expression for the ultimate soil resistance at moderate depth. The approach by Georgiadis (1983) was developed to incorporate determination of the ultimate soil resistance for layered soils in a Winkler model. This is done by introducing an equivalent system with fictive depths, x', for each of the soil layers. In this paper the approach is used to employ an equivalent system with a fictive depth of the sand layer to describe the effect of the overburden pressure.

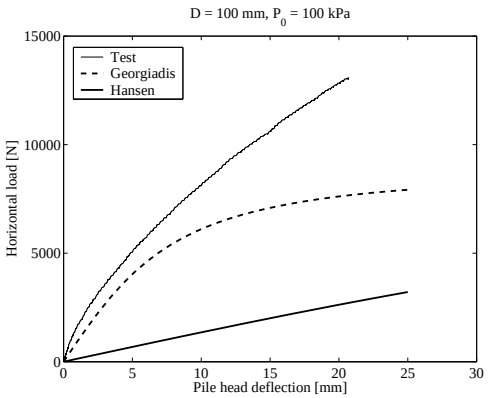

Figure 24: Load-deflection relationships measured at the level of the hydraulic piston (x = -370 mm) obtained from the tests and the Winkler model approach with the two expressions for the ultimate soil resistance accounting for the overburden pressure incorporated. D = 100 mm. P_0 = 100 kPa. The initial modulus of subgrade reaction, k, is set to 40000 kN/m^3.

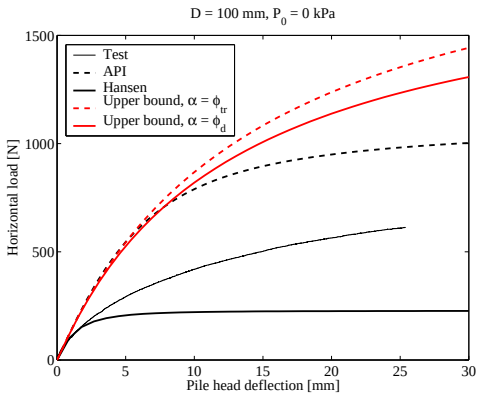

Figure 25: Load-deflection relationships measured at the height of the hydraulic piston (x = −370 mm) obtained from the tests and the Winkler model approach with the three different expressions for the ultimate soil resistance incorporated. D = 100 mm. P_0 = 0 kPa. The initial modulus of subgrade reaction, k, is set to 40000 kN/m^3.

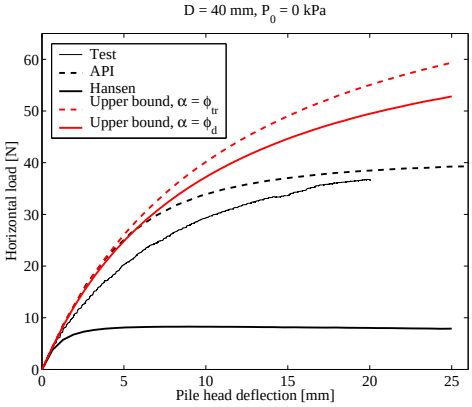

Figure 26: Load-deflection relationships measured at the height of the hydraulic piston (x = −370 mm) obtained from the tests and the Winkler model approach with the three different expressions for the ultimate soil resistance incorporated. D = 40 mm. P_0 = 0 kPa. The initial modulus of subgrade reaction, k, is set to 40000 kN/m^3.

In Fig. 24 the load-deflection relationship obtained by the two different methods are compared to the test results for the 100 mm pile with P_0 = 100 kPa. The figure shows that when employing the formulation given by Hansen (1961) the lateral load is significantly underestimated. The approach given by Georgiadis (1983) gives larger lateral load, but still, the load is underestimated. Thus, neither of the formulations are able to take the effect of the overburden pressure into account in a satisfactory way.

5.2 Evaluation of the Ultimate Soil Resistance

As none of the evaluated methods for incorporating the overburden pressure produced satisfactory results the evaluation of the ultimate soil resistance is based on the tests without overburden pressure. The expression for the ultimate soil resistance recommended by API (1993) is compared to two upper bound expressions given in Gwizdala and Jacobsen (1992) and Jacobsen (1989), respectively, and a lower bound solution given by Hansen (1961). The difference of the four expressions is the shape of the wedge formed in front of the pile, which is defined by the angle α. In API (1993), which is based on the formulation derived by Reese et al. (1974), $\alpha = \varphi_{tr}/2$. For the upper bound formulations $\alpha = \varphi_{tr}$ and $\alpha = \varphi_d$, the latter given by Eq. 4. For the lower bound formulation $\alpha = 0$.

$$\tan\varphi_d = \frac{\sin\varphi_{pl}\cdot\cos\psi}{1-\sin\varphi_{pl}\cdot\sin\psi} \qquad (4)$$

φ_d is the reduced angle of friction taking the energy loss into account in the kinematic admissible solution. $\varphi_{pl} = 1.1\cdot\varphi_{tr}$ is the plane angle of friction. The four expressions are incorporated in the Winkler model and the obtained load-deflection curves are shown in Figs. 25 and 26 together with the test results.

For the 100 mm pile with P_0 = 0 kPa, cf. Fig. 25, the ultimate soil resistance given by the horizontal asymptote of the curve is overestimated by both upper bound solutions. However the solution with the reduced angle of friction is seen to give the best estimate of the two. The lower bound solution is seen to underestimate the ulti-

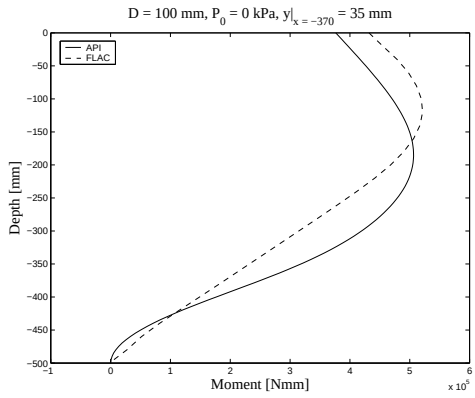

Figure 27: The moment curves obtained by means of the Winkler model approach with the ultimate soil resistance calculated by the design regulation formulation incorporated and the numerical model for D = 100 mm and P_0 = 0 kPa

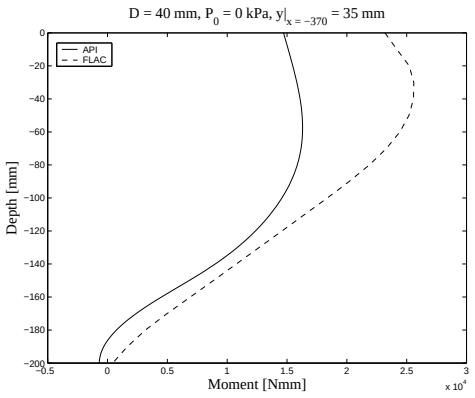

Figure 28: The moment curves obtained by means of the Winkler model approach with the ultimate soil resistance calculated by the design regulation formulation incorporated and the numerical model for D = 40 mm and P_0 = 0 kPa

mate soil resistance. The expression given in API (1993) predicts a lower capacity than the upperbound solutions but still the capacity is overestimated compared to the test results.

For the 40 mm pile the test results and the ultimate soil resistance determined according to API (1993) is found to be in better agreement, cf. Fig. 26. However, the deviation between the results for the 100 mm and the 40 mm pile must be seen in relation to the uncertainties when conducting the tests, where the largest uncertainties are related to the 40 mm pile, cf. Thomassen et al. (2010). Nevertheless, from the four expressions evaluated the expression given in API (1993) is found to give the best estimate of the ultimate soil resistance even though the results deviates from the laboratory tests.

6 Comparison of Design Regulations and Numerical Models

To establish whether the recommendations in the design regulations API (1993) and DNV (1992) gives good estimations of the pile-soil interaction for non-slender piles the design method and model results are compared. Again, only the results from the tests without overburden pressure are compared.

6.1 Evaluation of Bending Moment Distribution

The bending moment curves obtained from the numerical models are compared to the bending moment calculated by means of the Winkler model approach using the formulation for the ultimate soil resistances given by API (1993).

In Figs. 27 and 28 the moment curves for the 40 mm and 100 mm piles, respectively, are shown. Both curves are shown for a prescribed deflection of 35 mm at $x = -370$ mm. For both piles it can be seen that the maximum moment obtained by the numerical models is located approximately $1/5L$ below the soil surface. The maximum moment obtained from the Winkler approach is located approximately $2/5L$ below the soil surface. The maximum moments found by the numerical models are higher than the ones obtained by the Winkler model approach.

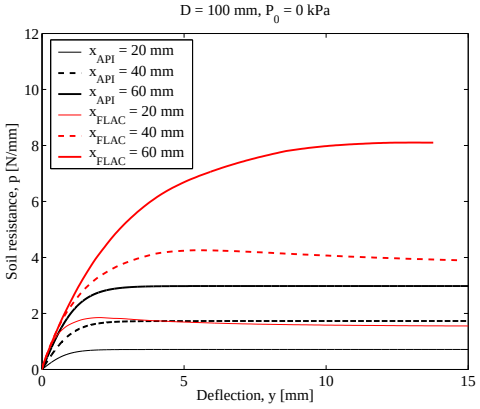

Figure 29: $p-y$ curves for three depths from the numerical model and the design regulation formulation for the 100 mm pile with P_0 = 0 kPa.

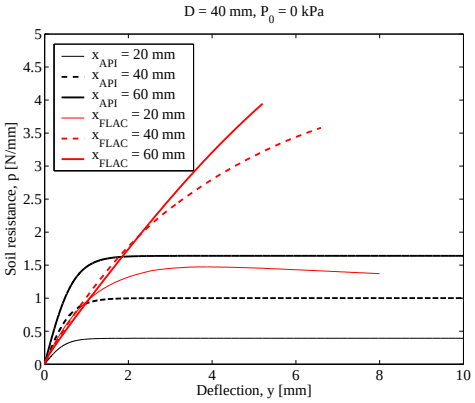

Figure 30: $p-y$ curves for three depths from the numerical model and the design regulation formulation for the 40 mm pile with P_0 = 0 kPa.

The maximum curvature of the moment-curves indicates the maximum soil pressure. At pile toe it can be seen that the moment obtained by means of API (1993) is curved whereas the modelled moment curve has no curvature. This indicates a difference in soil pressure and pile behaviour. Due to the differences between the measured and calculated moment distributions it is recommended that tests are carried out on piles instrumented with strain gauges in order to evaluate the correct behaviour of the pile.

6.2 Evalutation of p–y Curves

The $p-y$ curves recommended in the design regulations API (1993) and DNV (1992) are compared to the $p-y$ curves obtained by the numerical models. For the two tests without overburden pressure the comparison is shown in Figs. 29 and 30 for three different depths.

The figures show that the ultimate soil resistance recommended by API (1993) is significantly lower than the resistance obtained by the numerical models, most significant for the 40 mm pile, cf. Fig. 30. This large difference is believed to occur because the capacity in the numerical models are overestimated compared to the test results. Hence, the difference emerge from uncertainties when determining the soil parameters for low stress levels. In Fig. 30 the initial stiffness of the $p-y$ curves from the numerical models is seen to be in agreement with the calculated initial stiffness from the curve at a depth of 40 mm. In Fig. 29, however, the initial stiffness of the $p-y$ curves from the numerical models is in agreement with the calculated initial stiffness from the curve at 60 mm. Because the initial stiffness found by the numerical models are seen to be constant with depth, in the evaluated depth interval, and because of the difference in Fig. 29 and Fig. 30 it is difficult to draw any clear conclusions in relation to the recommendations other than the agreement between the curves are poor.

7 Evaluation of Initial Stiffness

In API (1993) and DNV (1992) the initial stiffness of the $p-y$ curves, E^*_{py} given by Eq. 5, is assumed to vary linearly with depth.

$$E^*_{py} = \frac{dp}{dy}|_{y=0} = k \cdot x \qquad (5)$$

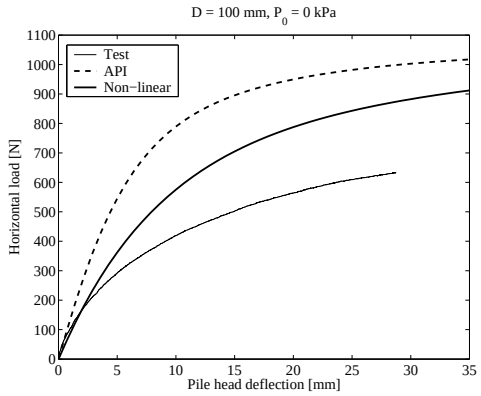

Figure 31: Load-deflection relation ships measured at the height of the hydraulic piston (x = -370 mm) obtained from the tests and the Winkler model approach with the expressions for the ultimate soil resistance with both linear and non-linear formulation of the initial stiffness incorporated. D = 100 mm. P_0 = 0 kPa. The initial modulus of subgrade reaction, k, is set to 40000 kN/m^3.

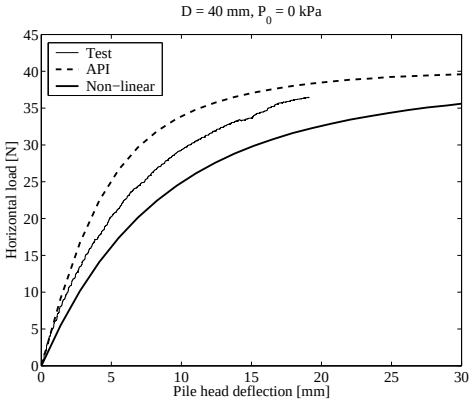

Figure 32: Load-deflection relation ships measured at the height of the hydraulic piston (x = -370 mm) obtained from the tests and the Winkler model approach with the expressions for the ultimate soil resistance with both linear and non-linear formulation of the initial stiffness incorporated. D = 40 mm. P_0 = 0 kPa. The initial modulus of subgrade reaction, k, is set to 40000 kN/m^3.

k is the initial modulus of subgrade reaction and x is the depth below soil surface. k is according to the design regulations dependent only on the relative density of the soil and, thus, independent of the pile properties.

Because of strict demands for the maximum rotation of the wind turbines and the resonance in serviceability mode the initial stiffness of the $p-y$ curves are of great importance. Therefore, it is of interest to find a correct expression for the initial stiffness in order to find the correct pile deflection. Sørensen et al. (2010) proposed a non-linear formulation for the initial stiffness, cf. Eq. 6, based on numerical simulations of full-scale monopiles in sand.

$$E_{py}^{*} = a\left(\frac{x}{x_{ref}}\right)^{b}\left(\frac{D}{D_{ref}}\right)^{c}\varphi_{tr}^{d} \qquad (6)$$

a is a factor determining E_{py}^{*} for (x,D,φ_{tr}) = (1 m, 1 m, 1 rad) and the constants (b,c,d) = (0.6, 0.5, 3.6), a = 50000 kN/m^2. x_{ref} and D_{ref} are reference values both of 1 m.

Similar to API (1993) the initial stiffness increases with increasing internal angle of friction, however, with a slightly different variation. Contrary to API (1993) the initial stiffness increases with increasing pile diameter and varies non-linearly with depth when using Eq. 6.

7.1 Comparison of Load-Deflection Relationships

Eq. 6 is inserted in the formulation for the soil resistance given in API (1993) and employed in the Winkler model. Thereby, the load-deflection relationships shown in Figs. 31 and 32 for the two piles without overburden pressure are obtained.

For the 40 mm pile, cf. Fig. 32, it is difficult to determine, which of the formulations gives the best fit to the test results as these results are positioned in between the two. Moreover, because of the large uncertainties for this test, the results may not be representative for the correct pile-soil behaviour.

The uncertainties for the test results with the 100 mm pile are smaller, and the results are considered more accurate. Fig. 31

shows that the formulation by API (1993) overestimates the lateral capacity. When using the non-linear formulation for the initial stiffness the lateral capacity is closer to the measured results, however, still overestimated. For the initial part of the curves, the non-linear expression is seen to be in better agreement with the results obtained in the laboratory tests and therefore the non-linear expression is believed to give the best estimate of the variation of the initial stiffness.

7.2 Comparison of p–y Curves

In order to evaluate the diameter effect the non-linear formulation, Eq. 6, for the initial stiffness is evaluated against the initial stiffness found from the $p-y$ curves from the six numerical models. The factor c is evaluated by the ratios:

$$\frac{E^*_{py}|_{D=100}}{E^*_{py}|_{D=40}} = \left(\frac{D_{100}}{D_{40}}\right)^c \qquad (7)$$

The initial stiffness of the numerically obtained $p-y$ curves, cf. Figs. 15, 16, and 17, is found by linear regression of the data until a deflection of approximately 0.2 mm. The slope of the linear regression is assumed representative for the initial stiffness, and the obtained values for the six models are shown in Tab. 4.

Table 4: The initial stiffness in N/mm^2 read of the $p-y$ curves obtained from the FLAC^{3D}-models for the two piles at different overburden pressures, cf. Figs. 15, 16, and 17.

	0 kPa	50 kPa	100 kPa
$E^*_{py}\|_{D=100}$	2.9	42.3	79.2
$E^*_{py}\|_{D=40}$	1.3	30.0	48.9

Table 5: Ratio of the initial stiffness of the $p-y$ curves obtained in the numerical models for the different overburden pressures.

	0 kPa	50 kPa	100 kPa
$\frac{E^*_{py}\|_{D=100}}{E^*_{py}\|_{D=40}}$	2.3	1.4	1.6

With $c = 0.5$, as proposed by Sørensen et al. (2010), the right side of Eq. 7 gives approximately 1.6. If this value of c is correct the ratio on the left side of the equation should give values of approximately 1.6 as well. In Tab. 5 the ratios of the initial stiffness from the numerical models are given. It can be seen that the ratio for the models without overburden pressure deviates the most. The ratios for the models with overburden pressure indicates that $c = 0.5$ is an appropriate value for the diameter effect on the initial stiffness. The results in Tab. 5 indicate that larger uncertainties are related to the tests without overburden pressure and, hence, low stress levels in the soil.

8 Conclusion

In this paper the diameter effect on the pile-soil interaction is evaluated by means of results from small-scale laboratory tests, numerical models of the same test setup, and existing theory. In total six tests were carried out on piles with outer diameters of 40 mm and 100 mm, respectively, and a slenderness ratio L/D of 5. In four of the tests overburden pressures of 50 kPa and 100 kPa were applied. The tests were modelled in the numerical finite difference program FLAC^{3D}, and the models were calibrated against the obtained load-deflection relationships from the laboratory tests. From the numerical models $p-y$ curves for the six tests were obtained and used in a comparison with the recommended curves in the current design regulations. From the evaluations, the following conclusions can be drawn:

From the numerical models the recorded deflection along the pile when subjected to lateral loading showed an increase in flexible behaviour when overburden pressure was applied. However, the primary deflection of the piles were caused by rigid body rotation.

To take the overburden pressure into account in the Winkler model approach formulations proposed by Hansen (1961) and Georgiadis (1983) was evaluated. However, none of the formulations produced results in agreement with the test results.

By means of the Winkler model approach the formulations for the ultimate soil resistance given by API (1993), Hansen (1961), Gwizdala and Jacobsen (1992), and Jacobsen (1989) were compared to the load-deflection relationships obtained from the laboratory tests without overburden pressure. The comparison showed that the formulation given by the current design regulation API (1993) provided the best agreement to the test results even though the ultimate resistance was overestimated.

Based on a comparison of the $p-y$ curves for the two pile diameters it was found that the initial stiffness, E^*_{py}, is dependent on the pile diameter, i.e. the initial stiffness increases with increasing pile diameter. Further, the $p-y$ curves obtained in the numerical models indicated that E^*_{py} is dependent on the stress state as E^*_{py} increases with increasing soil pressure along the pile and decreases with decreasing soil pressure.

The dependency of the diameter was evaluated by means of E^*_{py} obtained in the numerical models and by the non-linear formulation suggested in Sørensen et al. (2010). The models with overburden pressure indicated that a value of $c = 0.5$ for the diameter dependency is an appropriate value. By employing the formulation in a Winkler model approach the non-linear formulation was compared to the tests results and it was found that this formulation was in better agreement with the results than the formulations given in API (1993) and DNV (1992) where E^*_{py} is assumed independent of pile diameter.

From the calibration of the numerical models, the evaluation of $p-y$ curves, and the evaluation of E^*_{py} it was found that considerable uncertainties are related to small-scale testing and the different evaluations clearly indicates that the accuracy in small-scale testing is increased when increasing pile diameter and applying overburden pressure.

9 Acknowlegdements

The project is associated with the EFP programme "Physical and numerical modelling of monopile for offshore wind turbines", journal no. 033001/33033-0039. The funding is sincerely acknowledged.

Bibliography

API (1993), *Recommended Practice for Planning, Designing and Constructing Fixed Offshore Platforms – Working Stress Design*, American Petroleum Institute.

Brødbæk, K., Møller, M., Sørensen, S. and Augustesen, A. (2009), 'Evaluation of p-y relationship in cohesionless soil', *DCE Technical Report No. 57* . Aalborg University.

DNV (1992), *Foundations*, Det Norske Veritas. Classification Notes No. 30.4.

Georgiadis, M. (1983), 'Development of p-y curves for layered soils', *Proceedings of the Conference on Geotechnical Engineering* pp. 536–545.

Gwizdala, K. and Jacobsen, M., eds (1992), *Bearing capacity and settlements of piles*, Aalborg University. ISBN 87-88787-10-9.

Hansen, J. B. (1961), 'The Ultimate Resistance of Rigid Piles Against Transversal Forces', *Bulletin No. 12* . Geoteknisk Institut.

Ibsen, L. B., Hanson, M., Hjort, T. and Thaarup, M. (2009), 'MC-Parameter Calibration for Baskarp Sand No. 15', *DCE Technical Report No.62* . Department of Civil Engineering, Aalborg University.

Jacobsen, M. (1989), *Lærebog i videregående Geotektik 1, Brud i Jord.*

Lesny, K. and Wiemann, J. (2006), 'Finite-Element-Modelling of Large Diameter Monopiles for Offshore Wind Energy Converters', *Geo Congress* .

Poulos, H. and Hull, T. (1989), 'The Role of Analytical Geomechanics in Foundation Engineering', *Foundation Engineering: Current principles and practice, 2* pp. 1578–1606.

Reese, L. C., Cox, W. R. and Koop, F. D. (1974), 'Analysis of Laterally Loaded Piles in Sand', *Offshore Technology Conference* . Paper Number OTC 2080.

Sørensen, S., Ibsen, L. and Augustesen, A. (2010), 'Effects of diameter on initial stiffness of p-y curves for large-diameter piles in sand'. Aalborg University.

Sørensen, S., Møller, M., Brødbæk, K., Augustesen, A. and Ibsen, L. (2009), 'Numerical Evaluation of Load-Displacement Relationships for Non-Slender Monopiles in Sand', *DCE Technical Report No. 80* . Aalborg University.

Thomassen, K., Roesen, H. R., Ibsen, L. and Sørensen, S. (2010), 'Small-Scale Testing of Laterally Loaded, Non-Slender Monopiles in Sand', Short Candidate Project.

Recent publications in the DCE Technical Report Series

Brødbæk, K. T., Møller, M., Sørensen, S. P. H. and Augustesen, A. H. (2009) *Review of p-y relationships in cohesionless soil*, DCE Technical Report No. 57, Aalborg University. Department of Civil Engineering.

Sørensen, S. P. H., Møller, M., Brødbæk, K. T., Augustesen, A. H. and Ibsen, L. B. (2009) *Evaluation of Load-Displacement Relationships for Non-Slender Monopiles in Sand*, DCE Technical Report No. 79, Aalborg University. Department of Civil Engineering.

Sørensen, S. P. H., Møller, M., Brødbæk, K. T., Augustesen, A. H. and Ibsen, L. B. (2009) *Numerical Evaluation of Load-Displacement Relationships for Non-Slender Monopiles in Sand*, DCE Technical Report No. 80, Aalborg University. Department of Civil Engineering.

Thomassen, K., Roesen, H. R., Ibsen, L. B. And Sørensen, S. P. H. (2010) *Small-Scale Testing of Laterally Loaded Non-Slender Monopiles in Sand*, DCE Technical Report No. 90, Aalborg University. Department of Civil Engineering.

ISSN 1901-726X
DCE Technical Report No. 91